Experimental and Numerical Investigation of Particle Transport in a Horizontal Pipe

Robert Rundqvist, Camilla Ljus, and Berend van Wachem
Dept. of Thermo and Fluid Dynamics, Chalmers University of Technology, S-412 96 Göteborg, Sweden

DOI 10.1002/aic.10571
Published online September 2, 2005 in Wiley InterScience (www.interscience.wiley.com).

Measurements were made of the concentration of particles in a horizontal transport pipe using an optical probe. The distribution of particles over the pipe cross-section was measured. Particle transport in a horizontal two-dimensional (2-D) channel was simulated using an Eulerian two-fluid model. A model is proposed for the turbulent dispersion of particles and implemented in the two-fluid model. The turbulence in the gas phase is modeled using a modified $k - \varepsilon$ model that accounts for the influence of the particles on the gas-phase turbulence. Comparisons with measurements of air-particle flow in a horizontal pipe show qualitative agreement between measurements and calculations. © 2005 American Institute of Chemical Engineers *AIChE J,* 51: 3101–3108, 2005
Keywords: air-particle flow, two-fluid model, particle dispersion, turbulence modification, channel flow

Introduction

Particle transport by fluids is a common process in nature and in technical applications. Examples of such two-phase flows are mixing in bioreactors, the spreading of small particles in the atmosphere, transport of particles through pipes and channels, separation in cyclones and sediment transport in rivers and oceans. In some cases, such as pneumatic conveying, the transport of particles is strongly influenced by turbulence. Thus, turbulent dispersion must be accounted for when the distribution of particles is calculated. Studies of pneumatic conveying show that there is a minimum mean velocity at which particles can be transported through a horizontal pipe or a channel without being deposited on the pipe bottom. Predictions for this minimum velocity have been derived and discussed by, for example, [1–4]. At lower velocities the turbulent velocity will not be high enough to carry the particles and they will accumulate at the lower pipe wall. This indicates that, to avoid this accumulation, turbulent dispersion must be great enough to counteract the influence of gravity on the particles. When numerical calculations are made of these kinds of flows, it is necessary to include models for the turbulent dispersion force to obtain a particle distribution over the pipe cross-section. If no such force is included, all particles will eventually accumulate at the lower wall of the pipe. Most studies of particle transport in horizontal channels and pipes are experimental or analytical investigations. There are few studies in the literature in which the flow fields and the particles' distribution have been calculated numerically. [5] Made numerical calculations of pneumatic conveying. Their study includes particle-wall collisions but neglects turbulent dispersion of particles because of the large particle size. [6] Studied particle transport in horizontal pipes and included effects of turbulent dispersion, particle-particle and wall-particle collisions. The two-way coupling between the particles and the gas-phase turbulence was also modeled. A Lagrangian approach was used in both these investigations for the particle phase, for example, each particle is traced through the flow field. [7] Claimed to have made Eulerian calculations of gas-particle flow in a horizontal pipe. The gravitational force is neglected, however, and the turbulent dispersion is not included in the model. While the Eulerian approach was also used in calculations in horizontal, vertical, and inclined pipelines by [8], turbulent dispersion was not discussed.

The presence of particles in turbulent fluid flow may alter the turbulence intensity and the structure of turbulence. Experi-

Correspondence concerning this article should be addressed to R. Rundqvist at robert.rundqvist@fcc.chalmers.se

mental work by, for example, [9–12] showed that the presence of particles might either increase or decrease the turbulence levels depending on the size of the particles. Small particles increase the dissipation of turbulent energy, and large particles can cause additional turbulent production. Intermediate sized particles can have either effect, depending on which part of the flow field is studied. The length scales of the turbulence may also be affected, since a redistribution of energy between different wave numbers can occur, cf. for example, [13–15]. Many attempts have been made to model turbulence modification phenomena numerically, for example, [16–21]. However, there is still room for improvement since many of the models are simplified and apply only to certain flow cases, for example, small particles, no additional production, and noslip velocity. To be able to develop better turbulence models that capture correct turbulence behavior in particulate flows, it is necessary to understand the two-way coupling between the particles and the turbulence.

In this work, numerical calculations of particles transport in airflow in a horizontal, two-dimensional channel were made using an extended Eulerian two-fluid model that takes into account turbulent dispersion and turbulence modification. In earlier work predictions of particle distribution over the cross-section of a horizontal channel or pipe, using Eulerian models, have not been presented. The reason for this is believed to be the difficulty to take the turbulent dispersion, that is necessary to counteract gravity, into account in such a model.

To verify the models, measurements were made of the particle volume fraction profile of an air/particle suspension in a horizontal pipe. Comparisons were also made with previous measurements of gas velocity profiles in the same pipe, cf. [22]. Horizontal gas particle flows have previously been studied experimentally by for instance, [9] who studied a horizontal pipe flow with air and 0.2 mm particles using a laser doppler anemometer. They obtained velocity profiles for both phases using thresholding techniques. [23] Studied particle-wall interaction with spherical and rough particles using particle image velocimetry. As the work was focused on wall interaction, primarily impact and rebound characteristics of particles close to the walls were measured. [24] Studied particle-particle and particle-wall interaction with spherical glass beads in a horizontal channel air flow using a phase doppler anemometer. They measured air and particle mean velocity profiles, as well as first-order moments and particle volume fraction profiles.

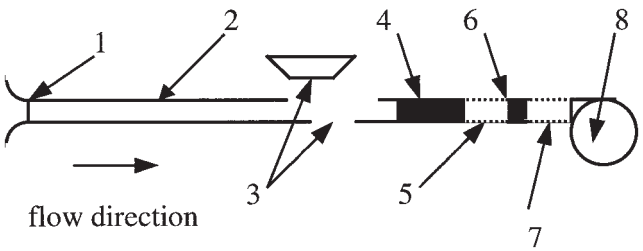

Figure 1. Experimental test rig: 1. Smoothly shaped inlet section, 2. Aluminium pipe, 3. Removable pipe section, 4. Venturi tube, 5. Plexiglas section, 6. "Étoile" straightener, 7. Bellow, 8. Fan.

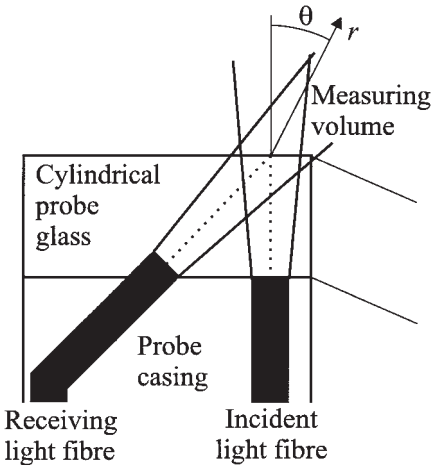

Figure 2. Probe tip geometry.

Experimental

Experimental setup

Experimental setup is shown in Figure 1. The particle volume fraction profile was measured in a horizontal aluminum pipe 10 m long and 0.108 m in dia. A classical Venturi tube with a machined convergent section with a dia. ratio of 0.75, designed according to the ISO 5167-1 standard, was used to measure the mean velocity. At low particle concentrations the extra pressure drop over the Venturi tube due to particles in the flow is negligible. The suction fan was set to give a mean gas velocity of 12 m/s. As particles were introduced, the gas velocity dropped and the fan was adjusted to keep the original velocity. The particles were injected at the inlet with a loading ratio of 0.1. The particles used were poly-acrylate particles having a diameter of 0.4 mm. The density of the particles is 1,000 kg/m^3. An optical probe, described in the next section, was traversed vertically along the pipe diameter, close to the end of the pipe. Measurements were made both from the top and the bottom of the test section in order to get a profile for the entire pipe diameter. The probe introduces incoherent infrared light into the measuring volume by an optical fiber. Another fiber adjacent to the introducing fiber, slanted by 45 degrees to limit the measuring volume, is used to receive the reflected light from the particles. The configuration of the fibers in the probe is shown in Figure 2.

Optical probe

The particle volume fraction in dilute flows can be measured by using several different measuring techniques. We chose to work with an optical probing technique, which is a simple but reliable method for measuring volume fraction profiles in confined flows. The probe uses infrared light from a diode that is transmitted into the flow orthogonally to the main flow direction by an optical fiber. Another fiber, slanted by 45 degrees, receives light reflected by the particles. This configuration keeps the measuring volume finite while minimising reflection disturbances. The probe has been manufactured at the department, more details of the technical specifications can be found in [25].

The main problem in using optical probe techniques for measuring particle volume fraction is the calibration, cf. for example, [25–28]. The method described in the last three refer-

ences is a straightforward procedure to apply, and as the volume fractions measured in this work are very low, the theory is clearly applicable. The method is based on the assumption that most of the light reaching the receiving fiber is scattered on a single particle. That is, light paths reflecting on more than one particle are neglected. This is a good approximation, especially at low particle volume fractions. There is, however, some uncertainty with respect to the influence of glare points on the calibration function. For smooth particles, the light from the probe will form a glare point on the particles, and the size of this glare point will vary with the distance to the probe, influencing the calibration function. If the particles are rough, there will be no glare point and the calibration function will be different than if smooth particles were used. In this case, the situation was even more complicated as the particles were found to be partially transparent as well as uneven in shape and roughness, which made determination of the optical qualities necessary for a successful calibration a difficult task.

In the dilute limit of the flow through the measuring volume, every particle will contribute to the registered signal. As the particle volume fraction increases, some particles will be hidden by other particles. This will introduce nonlinearity in the calibration function. There is however a range in the dilute region in which this effect is negligible and the calibration function can be considered linear. With the present probe and the given particle diameter, this linear range extends to a volume fraction of about 0.01, depending somewhat on whether a glare point is present. This justifies the use of a linear calibration function, where the proportionality factor is determined using the numerical calculations.

Numerical

Two-fluid model

The Eulerian two-fluid model used in this work is based on the "traditional" forms of the continuity and momentum equations, cf. for example, [29–31]. The basic form of the Reynolds decomposed and volume averaged continuity and momentum equations are

$$\frac{\partial}{\partial t}(\alpha_k \rho_k) + \frac{\partial}{\partial x_j}(\alpha_k \rho_k U_{kj}) = 0 \tag{1}$$

$$\frac{\partial}{\partial t}(\alpha_k \rho_k U_{ki}) + \frac{\partial}{\partial x_j}(\alpha_k \rho_k U_{ki} U_{kj}) = -\alpha_k \frac{\partial}{\partial x_j}(\delta_{ij} P) + M^d_{kIi} + \alpha_k \rho_k g_i + C_{ki} + V_{ki} \tag{2}$$

where the phase index k is g for the gas phase and p for the particle phase, α_k is the average volumetric occurrence of phase k, ρ_k is the density, U_{ki} is the velocity, P is the gas-phase pressure, M^d_{kIi} is the generalised drag, g_i is the gravitational acceleration, V_{ki} is the viscous force, and C_{ki} represents the particle-particle interaction force, which is zero in the gas phase. These are the laminar forms of the transport equations. The equations including the additional terms that take turbulence into account are presented below in this paragraph. A number of closure equations are also needed. The gas density is calculated using the ideal gas law. The particle-particle interaction force is assumed to be zero at the low-particle concentrations used in this study. The generalised drag is contributed to by stationary drag, added mass, transverse, history, and other forces. For suspensions with a small gas-to-particle density ratio, the only force included in the two-fluid model is normally the stationary drag, while the remaining forces are neglected. The generalised drag can then be written

$$M^d_{kIi} = \begin{cases} K(U_{pi} - U_{gi}) & \text{if } k = g \\ K(U_{gi} - U_{pi}) & \text{if } k = p \end{cases} \tag{3}$$

For a dispersed flow, the generalised drag force per unit volume in a suspension of particles is written

$$M^d_{kIi} = n_p F^{dr}_i \tag{4}$$

where the number of particles per unit of volume, n_p, is

$$n_p = \frac{\alpha_p}{V_p} \tag{5}$$

The volume of a particle is here denoted V_p. The drag force on a spherical particle can be written

$$F^{dr}_{sp} = \frac{1}{2} C^{sp}_d \rho_g U_r U_r \frac{\pi d_p^2}{4} \tag{6}$$

where d_p is the particle diameter and U_r is the relative velocity between the phases. The drag function used here for spherical particles is that given by [32]

$$C^{sp}_d = \begin{cases} \dfrac{24}{\mathrm{Re}_d}(1 + 0.15(\mathrm{Re}_d)^{0.687}) & \text{if } \mathrm{Re}_d < 1000 \\ 0.44 & \text{if } \mathrm{Re}_d > 1000 \end{cases} \tag{7}$$

Here, Re_d is the Reynolds number based on the particle diameter and the relative velocity between the phases.

The viscous force in the momentum equation is given by

$$V_{ki} = \frac{\partial}{\partial x_j}(\alpha_k \tau_{kij}) \tag{8}$$

The stress tensor is modeled using the Newtonian strain-stress relation

$$\tau_{kij} = \xi_k \left(\frac{\partial U_{kl}}{\partial x_l} \right) \delta_{ij} + 2\mu_k \left(S_{kij} - \frac{1}{3} \left(\frac{\partial U_{kl}}{\partial x_l} \right) \delta_{ij} \right) \tag{9}$$

and the strain-rate tensor is defined by

$$S_{kij} = \frac{1}{2} \left(\frac{\partial U_{ki}}{\partial x_j} + \frac{\partial U_{kj}}{\partial x_i} \right) \tag{10}$$

where μ_k is the dynamic viscosity of phase k. For dilute suspensions, the bulk viscosity of phase k, ξ_k, is often set to

zero in both phases, in accordance with Stokes' assumption, cf. for example, [33]. This work, the particulate phase viscosity is set to zero, as the particle concentration is very low and the particulate phase viscosity decreases with decreasing concentration.

If turbulence is taken into account, Eqs. 1 and 2 will have additional terms that can be obtained by Reynolds decomposing and time averaging of the equations, cf. for example, [18,20,34]. These additional terms will, for example, be correlations between fluctuating velocities and fluctuating particle concentration.

When these terms are included, the continuity equation for the particulate phase, for steady-state mean flow, can be written

$$\frac{\partial}{\partial x_i}\left(\alpha_p U_{pi} + \overline{\alpha'_p u'_{pi}}\right) = 0 \tag{11}$$

where α'_p and u'_p are the fluctuating particle concentration and the fluctuating particle velocity, respectively. Another approach is to apply mass-weighted averaging or Favre averaging. A Favre-averaged variable is given by

$$\widetilde{\Phi_k} = \frac{\overline{\alpha_k \rho_k \Phi_k}}{\overline{\alpha_k \rho_k}} \tag{12}$$

Neglecting density fluctuations, a relationship between time the averaged, and the Favre averaged can be obtained

$$\widetilde{\Phi_k} = \overline{\Phi_k} + \frac{\overline{\alpha'_k \Phi'_k}}{\overline{\alpha_k}} \tag{13}$$

Using Eqs. 11 and 13, the Favre-averaged continuity equation becomes

$$\frac{\partial}{\partial x_i}\left(\overline{\alpha_p}\widetilde{U_{pi}}\right) = 0 \tag{14}$$

This means that there is no additional term in the continuity equation due to the turbulence. There will, however, be additional terms in the momentum equations. The Favre-averaged equations are written as

$$\frac{\partial \overline{\rho_k \alpha_k}}{\partial t} + \frac{\partial}{\partial x_i}\left(\rho_k \overline{\alpha_k}\widetilde{U_{gi}}\right) = 0 \tag{15}$$

$$\frac{\partial}{\partial t}\left(\rho_g \overline{\alpha_g}\widetilde{U_{gi}}\right) + \frac{\partial}{\partial x_j}\left(\rho_g \overline{\alpha_g}\widetilde{U_{gi}}\widetilde{U_{gj}}\right) = -\overline{\alpha_g}\frac{\partial}{\partial x_j}(P\delta_{ij}) - \bar{K}\left[(\widetilde{U_{gi}} - \widetilde{U_{pi}}) + \frac{\overline{\alpha'_g u'_{gi}}}{\overline{\alpha_g}} - \frac{\overline{\alpha'_p u'_{pi}}}{\overline{\alpha_p}}\right] + \frac{\partial}{\partial x_j}\left(\overline{\alpha_g}\tau_{gij} - \rho_g \overline{\alpha_g u'_{gi} u'_{gj}}\right) + \overline{\alpha_g}\rho_g g_i \tag{16}$$

$$\frac{\partial}{\partial t}\left(\rho_p \overline{\alpha_p}\widetilde{U_{pi}}\right) + \frac{\partial}{\partial x_j}\left(\rho_p \overline{\alpha_p}\widetilde{U_{pi}}\widetilde{U_{pj}}\right) = -\overline{\alpha_p}\frac{\partial}{\partial x_j}(P\delta_{ij}) - \bar{K}\left[(\widetilde{U_{pi}} - \widetilde{U_{gi}}) + \frac{\overline{\alpha'_p u'_{pi}}}{\overline{\alpha_p}} - \frac{\overline{\alpha'_g u'_{gi}}}{\overline{\alpha_g}}\right] + \frac{\partial}{\partial x_j}\left(\overline{\alpha_p}\tau_{pij} - \rho_p \overline{\alpha_p u'_{pi} u'_{pj}}\right) + \overline{\alpha_p}\rho_p g_i \tag{17}$$

Here, higher-order correlations are neglected. Correlation $\overline{\alpha'_k u'_{ki}}$ can be modeled using a gradient diffusion model

$$\overline{\alpha'_k u'_{ki}} = -\nu_{tk}\frac{\partial \overline{\alpha_k}}{\partial x_i} \tag{18}$$

Here, ν_{tk} is a diffusion coefficient for phase k, which can also be regarded as a "turbulent viscosity."

The Reynolds stresses in the gas phase, $\overline{u'_{gi} u'_{gj}}$, are modeled using the Boussinesq assumption

$$-\overline{u'_{gi} u'_{gj}} = \nu_{tg}\left(\frac{\partial \widetilde{U_{gi}}}{\partial x_j} + \frac{\partial \widetilde{U_{gj}}}{\partial x_i}\right) - \frac{2}{3}\delta_{ij}k \tag{19}$$

where k is the turbulent kinetic energy in the gas phase

$$k = \frac{1}{2}\overline{u'_{gi} u'_{gi}} \tag{20}$$

The turbulent viscosity of the gas phase can be calculated from the turbulent kinetic energy k, and the rate of dissipation, ε using the following relation

$$\nu_{tg} = C_\mu \frac{k^2}{\varepsilon} \tag{21}$$

where $C_\mu = 0.09$. The Boussinesq assumption extended to the particulate phase, according to [18], can be written

$$-\overline{u'_{pi} u'_{pj}} = \nu_{tp}\left(\frac{\partial \widetilde{U_{pi}}}{\partial x_j} + \frac{\partial \widetilde{U_{pj}}}{\partial x_i}\right) - \frac{2}{3}\delta_{ij}\left(k_p + \nu_{tp}\frac{\partial \widetilde{U_{pl}}}{\partial x_l}\right) \tag{22}$$

where k_p is the turbulent kinetic energy in the particulate phase

$$k_p = \frac{1}{2}\overline{u'_{pi} u'_{pi}} \tag{23}$$

The last term in Eq. 22 is required to give Eq. 22 the correct trace, that is to ensure that Eq. 23 is valid.

The additional term in the drag force in Eqs. 16 and 17 that

occurs from fluctuating velocities and particle concentration can be interpreted as a drag force on the particles by the fluctuating gas velocity.

A number of models for the "turbulent viscosity" of the particulate phase have been suggested in the literature, cf. for example, [19–20]. Their models are all rather similar, with a dependence on the turbulent viscosity of the gas phase ν_{tg}, the particle response time τ_m, and the Lagrangian time integral scale T_L. The model of [18], however, can give negative ν_{tp} values for pipe flow. The present calculations use the model of [20]:

$$\nu_{tp} = \nu_{tg} \frac{1}{1 + \frac{\tau_m}{T_L}} \tag{24}$$

Comparing the drag term in the model by [18] with the drag term in Eq. 2, the particle response time can be written

$$\tau_m = \frac{\alpha_p \rho_p}{K}. \tag{25}$$

The Lagrangian integral time scale is given by [18]

$$T_L = 0.41 \frac{k}{\varepsilon} \tag{26}$$

Turbulence model

In this work, the turbulence model for the gas-phase is a modified $k - \varepsilon$-model based on the model by [18]. In their model, the additional dissipation caused by the particles is taken into account but the additional production due to the particles is neglected. In the present work a term taking into account the additional production caused by the larger particles is also included. This wake production P_{kp}, becomes important when the size of the particles is large in comparison to the turbulent scale. The transport equations for the turbulent kinetic energy k, and the dissipation rate ε, in the gas phase can be written

$$\frac{\partial(\overline{\alpha_g}\rho_g k)}{\partial t} + U_{gj}\frac{\partial(\overline{\alpha_g}\rho_g k)}{\partial x_j} = \frac{\partial}{\partial x_j}\left(\frac{\nu_{tg}}{\sigma_k}\frac{\partial(\overline{\alpha_g}\rho_g k)}{\partial x_j}\right) + \overline{\alpha_g}\rho_g(P_k - \varepsilon + P_{kp} - \varepsilon_p) \tag{27}$$

$$\frac{\partial(\overline{\alpha_g}\rho_g \varepsilon)}{\partial t} + U_{gj}\frac{\partial(\overline{\alpha_g}\rho_g \varepsilon)}{\partial x_j} = \frac{\partial}{\partial x_j}\left(\frac{\nu_{tg}}{\sigma_\varepsilon}\frac{\partial(\overline{\alpha_g}\rho_g \varepsilon)}{\partial x_j}\right) + \overline{\alpha_g}\rho_g\left[\frac{\varepsilon}{k}(C_1 P_k - C_2\varepsilon) - e_p\right] \tag{28}$$

where P_k is the production of turbulence by the velocity field

$$P_k = -\overline{u'_{gi}u'_{gj}}\frac{\partial \widetilde{U_{gi}}}{\partial x_j} \tag{29}$$

Term ε_p is the additional dissipation owing to the particles, that is, the turbulent kinetic energy transfer to the particulate phase, and e_p is an additional term that takes into account the influence of particles on gas-phase dissipation. By deriving the transport equations for k and ε for dilute suspensions, [35] obtains the following expressions for ε_p and e_p, respectively

$$\varepsilon_p = \frac{\bar{K}}{\rho_g}\left[\overline{u'_{gi}u'_{gi}} - \overline{u'_{gi}u'_{pi}} + \frac{1}{\alpha_p}\overline{\alpha'_p u'_{gi}}(\widetilde{U_{gi}} - \widetilde{U_{pi}})\right] \tag{30}$$

$$e_p = \frac{\bar{K}}{\rho_g}\left[\varepsilon - \nu\overline{\frac{\partial u'_{gi}}{\partial x_j}\frac{\partial u'_{pi}}{\partial x_j}}\right] \tag{31}$$

Term e_p is a correlation between the fluctuating gas strain rate and the strain associated with the fluctuating slip velocity. A derivation by [35] shows that e_p can be modeled

$$e_p = \frac{\bar{K}}{\rho_g}\left[\varepsilon - \nu\left[\frac{\varepsilon}{\nu}\frac{T_L}{\tau_m + T_L} + \frac{\tau_m}{(\tau_m + T_L)^2}\frac{\partial k}{\partial x_j}\frac{\partial T_L}{\partial x_j}\right]\right]. \tag{32}$$

By considering the limiting behavior of correlation $\overline{u'_{gi}u'_{pi}}$ in the limits of small and large values of τ_m/T_L, that is, the limits of perfectly responsive particles and nonresponsive particles, respectively, the correlation, according to [35], can be written

$$\overline{u'_{gi}u'_{pi}} = 2k\frac{T_L}{\tau_m + T_L} \tag{33}$$

Using similar reasoning, the turbulent kinetic energy of the particulate phase k_p, is modeled as

$$k_p = k\frac{T_L}{\tau_m + T_L} \tag{34}$$

Constants σ_k, σ_ε, C_1, and C_2 are set to the values used for a standard $k - \varepsilon$-model in single-phase flow, that is, 1.0, 1.3, 1.44, and 1.92 respectively, cf. for example, [36].

The model by [18] does not take into account the additional production that larger particles can cause. Several models for wake production can be found in the literature, most of which can be written in the form

$$P_{kp} = f(|\widetilde{U_{gi}} - \widetilde{U_{pi}}|)^2 \tag{35}$$

where f may be a function of particle response time, particle size, wake size, particle and fluid density, and drag coefficient. [37] Derived the turbulence energy equation for the gas phase in the presence of particles based on the volume averaging of the mechanical energy equation of the gas phase. The derivation gives a k-equation with additional terms for both the dissipation caused by particles, and the production caused by particles. The production term, which was used in the present study, can be written

$$P_{kp} = \frac{K}{\rho_g}(|\widetilde{U_{gi}} - \widetilde{U_{pi}}|)^2 \tag{36}$$

This means that the production of turbulent energy will be dependent of the drag between particles and gas and the slip velocity, which will be larger for larger particles.

Numerical method

The densities of both phases are assumed to be constant and a solver for incompressible two-phase flow is used. A thorough description of the method is given by [38]. The transport equations for the turbulence are solved explicitly for each time step from the latest calculated velocity filed. From the k and ε fields, new turbulent viscosities for the two phases, and the turbulent kinetic energy for the particles phase are obtained. These are then used in the momentum equations for the next time step. The obtained solution will not completely stationary. The particles will buildup in the channel, and then be swept away from time to time. This will give a solution that will vary to a small extent in time, but the variations will be small. This is a true physical effect if the velocity of the gas is not high enough to keep all particles suspended. By integrating the velocity and concentration profile time-averaged profiles comparable to the measured profiles are obtained.

Calculations

The computational domain is a two-dimensional channel with a width of 0.1 m, and a length of 9.0 m. A coordinate system is chosen that has the x_1 axis along the length of the channel and the x_2 axis across the channel and directed upwards. The origin of the coordinate system is located at the lower wall at the inlet. The grid has 32 cells across the channel and 900 along the channel length. The grid is refined at the walls, and the wall cell is 0.77 mm in the x_2 direction, which is at y^+ between 30 and 40 for the present flow cases.

The horizontal walls are impermeable and a noslip condition is used for the gas phase. A partial slip condition given by

$$U_{p1} = L \frac{\partial U_{p1}}{\partial x_2} \tag{37}$$

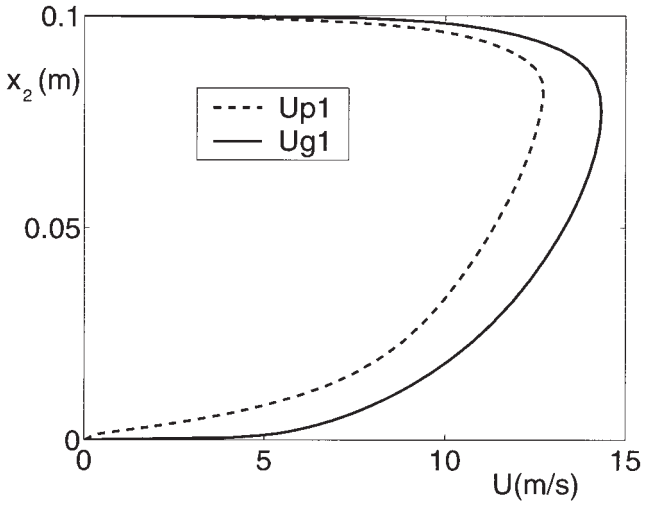

Figure 3. Calculated gas and particle velocity over pipe cross-section.

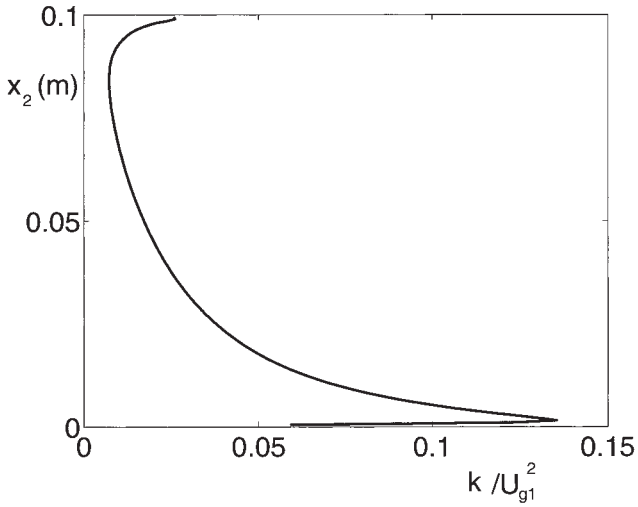

Figure 4. Calculated turbulent kinetic energy.

is applied to the particle phase. Here the slip parameter suggested by [39] is used

$$L = \frac{\Phi d_p}{6\sqrt{2}\,\alpha_p} \tag{38}$$

where Φ is the sphericity of the particles. The pressure and particle concentration derivatives are set to zero at the walls. The derivatives of the velocities, the particle concentration and the turbulent properties are set to zero at the outlet since the flow field is fully developed.

The wall boundary conditions for the k and ε equations are set by using standard wall functions based on the friction velocity u_*, cf. [36]. The influence of the particles on the law of the wall is not taken into account and the standard logarithmic profile is used. At the inlet, the turbulence intensity is set to a constant value of 1%.

The inlet mean velocity for the gas, and the particles is 12 m/s, and the loading ratio, that is, the ratio between the mass flow of the particles and the mass flow of the gas, is 0.1.

The spherical particles are poly-acrylate particles with a mean particle diameter of 450 μm and a density of 1,000 kg/m^3.

Results and Discussion

Measurements by, for example, [22] show that the velocity profile, and, therefore, also the particle concentration, is asymmetric in pipe flow at the particle loading used.

Figure 3 shows the calculated gas and particle velocities. The maximum velocity for the gas and particle phase is 14.3 m/s and 12.7 m/s, respectively. Both are clearly skewed towards the upper part of the pipe, and the slip velocity is relatively constant over the cross-section of the channel. This skewness is also apparent in the turbulent kinetic energy plot (Figure 4), where the local turbulent intensities are higher in the lower part of the pipe due to the lower gas velocity.

Figure 5 shows comparisons between measured and calculated particle volume fractions. The agreement is good, but there is a slight tendency toward stronger segregation in the measured profile. That is, the simulated profile is slightly more

evenly distributed. The main error sources are considered to be in the disturbance of the flow by the probe, as the noise levels in the signals are low and ca be neglected.

A comparison between the shapes of the measured and calculated gas velocities is shown in Figure 6. The measured gas velocity is obtained from an earlier experimental study of the same flow case by [22]. The mean velocity of the measured and calculated profiles are the same although the maximum velocity will differ because of the somewhat different shapes of the profiles. It is evident that the simulated profile is more skewed toward the upper part of the channel than the measured profile. This can be interpreted such that the particles absorb more of the gas phase momentum in the simulations than is the case in reality. This would force the simulated gas to move faster in the dilute upper regions, thereby skewing the profile. The explanation for the discrepancy may lie in one or more of the following four possible explanations:

1. The drag model over predicts the momentum transfer between the phases. This is unlikely, especially for such dilute suspensions. The interphase drag is one of the more thoroughly researched closures and, given the other uncertainties, the reason for this discrepancy should probably not be sought here.

2. The partial-slip boundary condition for the particle phase over predicts the momentum transfer from the particle phase to the wall. This will lead to a larger slip velocity and, thus, a larger momentum transfer between the phases.

3. The turbulent particle viscosity over predicts the momentum transfer from the particles to the wall. A lower viscosity would transport momentum less efficiently and, thus, reduce the slip velocity between the phases. This would also lead to a less skewed velocity profile.

4. The discrepancy is a physical effect of the difference between the simulated 2-D channel flow, and the 3-D pipe flow. In the pipe flow, the midsection contains relatively more momentum than the peripheral upper and lower regions, which could cause the midregion to act as a momentum buffer. As the particle phase drains momentum from the gas phase in the lower parts of the pipe flow, the core region can provide momentum without decelerating as much. This would imply that the 2-D channel velocity profile should be more skewed than the 3-D pipe flow.

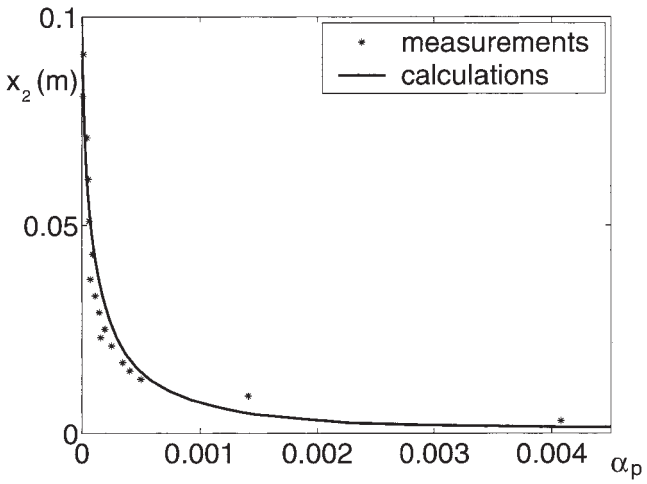

Figure 5. Particle distribution over the pipe cross-section.

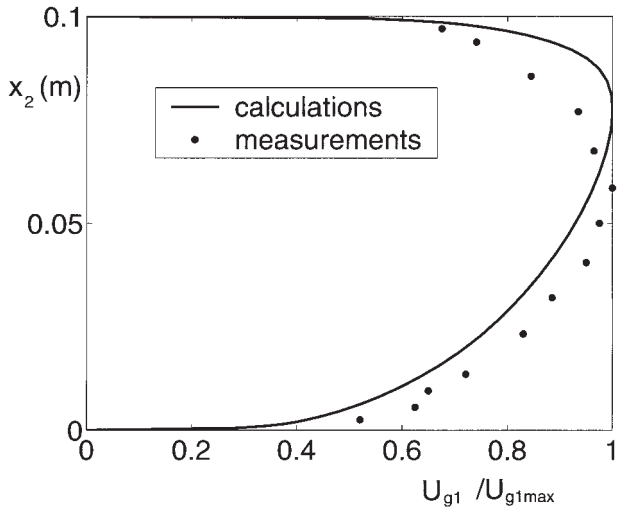

Figure 6. Measured and calculated gas velocity.

The correct explanation (or explanations) should be the subject of further investigation.

Conclusions

The agreement between model predictions and measurements is good. Further investigations should include a 3-D simulation of a horizontal flow.

Acknowledgments

The authors would like to thank the Swedish Foundation for Strategic Research (SSF) and SCA Research AB for financial support of this work.

Notation

C_1 = constant in $k-\varepsilon$-model
C_2 = constant in $k-\varepsilon$-model
C_d^{sp} = drag function for spherical particle
$C_d^{\perp}$ = drag function for straight fiber perpendicular to the velocity
C_d^{fib} = drag function for fiber
C_{ki} = particle-particle force, N/m^3
C_μ = constant in $k-\varepsilon$-model
D = dia. of test pipe, m
d_f = mean dia. of the fibers, m
d_p = mean dia. of the spherical particles, m
e_p = additional term in the ε equation due to the particle presence, m^2/s^4
F_i^{dr} = drag force on a single particle, N
$F_{\perp}^{dr}$ = drag force on fiber perpendicular to the velocity, N
F_{sp}^{dr} = drag force on spherical particle, N
f = function in wake production model, 1/s
K = drag function, kg/m^3 s
k = turbulent kinetic energy in the gas phase, m^2/s^2
k_p = turbulent kinetic energy in the particle phase, m^2/s^2
L = slip parameter according to [39], m
M_{kIi}^d = generalized drag, N/m^3
m = loading ratio
P = pressure, N/m^2
P_k = production of gas-phase turbulent energy by the mean velocity field, m^2/s^3
P_{kp} = additional production of gas-phase turbulent energy due to the particles, m^2/s^3
T_L = Lagrangian integral time scale, s
t = time, s
U_{gi} = mean gas velocity in the i direction, m/s
$\bar{U}_{in}$ = inlet mean velocity, m/s
U_{ki} = mean velocity of phase k in the i direction, m/s
U_{pi} = mean gas velocity in the i direction, m/s

U_r = relative velocity between the phases, m/s
u'_{gi} = fluctuating gas velocity, m/s
u'_{pi} = fluctuating particle velocity, m/s
V_{ki} = viscous force, N/m^3
V_p = volume of particle, m^3
x_i = coordinate, m
y^+ = dimensionless wall distance
α_p = mean particle volume concentration
α'_p = fluctuating particle volume concentration
β_1 = constant in the turbulent diffusion model, kg/ms^2
β_2 = constant in the turbulent diffusion model, kg/m^3
δ_{ij} = Kronecker delta
ε = rate of dissipation of the gas-phase turbulent energy, m^2/s^3
ε_p = rate of dissipation of the gas-phase turbulent energy due to particles, m^2/s^3
μ_k = dynamic viscosity of phase k, kg/ms
ν = kinematic viscosity of the gas phase, m^2/s
ν_{tg} = turbulent viscosity of the gas phase, m^2/s
ν_{tp} = turbulent viscosity of the particle phase, m^2/s
ξ_k = bulk viscosity of phase k, kg/ms
ρ_g = gas density, kg/m^3
ρ_p = particle density, kg/m^3
σ_ε = constant in $k - \varepsilon$-model
σ_{d1} = constant in the particle diffusion model
σ_{d2} = constant in the particle diffusion model
σ_k = constant in $k - \varepsilon$-model
τ_{kij} = stress tensor, N/m^2
τ_m = response time for the particles, s
Φ = sphericity of particles
$\widetilde{\Phi_k}$ = Favre averaged variable for phase k
$\overline{\Phi_k}$ = time-averaged variable for phase k

Literature Cited

1. Thomas AD. Predicting the deposit velocity for horizontal turbulent pipe flow of slurries. *Int J Multiphase Flow.* 1979;5:113–129.
2. Oroskar AR, Turian RM. The critical velocity in pipeline flow of slurries. *AIChE J.* 1980;26:550–558.
3. Davies JT. Calculation of critical velocities to maintain solids in suspension in horizontal pipes. *Chem Eng Sci.* 1987;42:1667–1670.
4. Cabrejos FJ, Klinzing GE. Pickup and saltation mechanisms of solid particles in horizontal pneumatic transport. *Powder Technol.* 1994;79: 173–186.
5. Tsuji Y, Oshima T, Morikawa Y. Numerical simulation of pneumatic conveying in a horizontal pipe. *KONA.* 1985;3:38–51.
6. Huber N, Sommerfeld M. Modelling and numerical calculation of dilute-phase pneumatic conveying in pipe systems. *Powder Technol.* 1998;99:90–101.
7. Hussainov M, Kartushinsky A, Mulgi A, Rudi Ü. Gas-solid flow with a slip velocity of particles in a horizontal channel. *J Aerosol Sci.* 1996;27:41–59.
8. Levy A, Mooney T, Marjanovic P, Mason DJ. A comparison of analytical and numerical models with experimental data for gas-solid flow through a straight pipe at different inclinations. *Powder Technol.* 1997;93:253–260.
9. Tsuji Y, Morikawa Y. LDV measurements of an aid-solid two-phase flow in a horizontal pipe. *J Fluid Mech.* 1982;120:385–409.
10. Rashidi M, Hetsroni G, Banerjee S. Particle-turbulence interaction in a boundary layer. *Int J Multiphase Flow.* 1990;16:935–949.
11. Kulick JD, Fessler JR, Eaton JK. Particle response and turbulence modification in fully developed channel flow. *J Fluid Mech.* 1994;227: 109–134.
12. Kaftori D, Hetsroni G, Banerjee S. The effect of particles on wall turbulence. *Int J Multiphase Flow.* 1998;24:359–386.
13. Tsuji Y, Morikawa Y, Shiomi H. LDV measurements of an air-solid two-phase flow in a vertical pipe. *J Fluid Mech.* 1984;139:417–434.
14. Sato Y, Hanzawa K, Maeda M. Interactions between particle wake and turbulence, in a water channel flow. in *Advances in Multiphase Flow.* Serizawa A, Fukano T, Bataille J, eds. Amsterdam: Elsevier Science; 1995.
15. Boivin M, Simonin O, Squires KD. Direct numerical simulation of turbulence modification by particles in isotropic turbulence. *J Fluid Mech.* 1998;375:235–263.
16. Dannon H, Wolfshtein M, Hetsroni G. Numerical calculations of two-phase turbulent round jet. *Int J Multiphase Flow.* 1977;3:223–234.
17. Elgobashi SE, Abou-Arab TW. A two-equation turbulence model for two-phase flows. *Phys Fluids.* 1983;26:931–938.
18. Pourahmadi F, Humphrey JAC. Modeling solid-fluid turbulent flows with application to predicting erosive wear. *Physico Chemical Hydrodynamics.* 1983;4:191–219.
19. Choi YD, Chung MK. Analysis of turbulent gas-solid suspension flow in a pipe. *J Fluids Eng.* 1983;105:329–334.
20. Chen CP, Wood PE. Turbulence closure modeling of two-phase flows. *Chem Eng Commun.* 1984;29:291–310.
21. Yokomine T, Shimizu A. Prediction of turbulence modulation by using $k - \varepsilon$ model for gas-solid flows. in *Advances in Multiphase Flow.* Serizawa A, Fukano T, Bataille J, eds. Amsterdam: Elsevier Science, 1995.
22. Ljus C, Johansson B, Almstedt AE. Turbulence modification by particles in a horizontal pipe flow. *Int J Multiphase Flow.* 2002;28:1075–1090.
23. Sommerfeld M, Huber N. Experimental analysis and modelling of particle-wall collisions. *Int J Multiphase Flow.* 1999;25:1457–1489.
24. Kussin J, Sommerfeld M. Experimental studies on particle behaviour and turbulence modification in horizontal channel flow with different wall roughness. *Exp in Fluids.* 2002;33:143–153.
25. Rundqvist R, Magnusson A, van Wachem BGM, Almstedt AE. Dual optical fibre measurements of the particle concentration in gas-solid flows. *Exp in Fluids.* 2003;35:572–579.
26. Bergougnoux L, Misguich-Ripault J, Firpo JL, André J. Monte Carlo calculation of backscattered light intensity by suspension: comparison with experimental data. *Applied Optics.* 1996;35:1735–1741.
27. Magnusson A. *Fluid dynamics of a Wurster-type fluidized bed.* Doctoral Thesis Dept. of Thermo and Fluid Dynamics. Chulmers University of Technology. Sweden. ISSN: 0346-718X. 2004.
28. Magnusson A, Rundqvist R, Almstedt AE, Johansson F. Dual fibre probe measurements of solid volume fraction in a circulating fluidized bed. In press: *Powder Technol.* 2005;151:1–3. 19.
29. Ishii M. *Thermo-Fluid Dynamic Theory of Two-Phase Flow.* Eyrolles; 1975.
30. Bouré JM, Delhaye JM. in *Handbook of Multiphase Systems.* Hetsroni G, ed. New York: McGraw-Hill; 1982.
31. Enwald H, Peirano E, Almstedt AE. Eulerian two-phase theory applied to fluidization. *Int J Multiphase Flow.* 1997;22:21–66.
32. Schiller L, Naumann ZZ. *Ver Deutsch Ing.* 1935;77:318.
33. Panton RL. *Incompressible Flow.* La Cañada, California: DCW Industries, Inc; 1984.
34. Chung MK, Sung HJ, Lee KB. Computational study of turbulent gas-particle flow in a venturi. *ASME trans.* 1986;108:248–252.
35. Pourahmadi F. *Turbulence modeling of single and two phase curved channel flow.* University of California, Berkeley, Department of Mechanical Engineering; 1982. PhD thesis.
36. Wilcox DC. *Turbulence Modeling for CFD.* La Cañada, California: DCW Industries, Inc; 1993.
37. Crowe CT, Gillandt I. Turbulence modulation of fluid-particle flows—a basic approach in *Third International Conference on Multiphase Flows;* France: Lyon; 1998.
38. Weller HG, Tabor G, Jasak H, Fureby C. A Tensorial Approach to Computational Continuum Mechanics Using Object Orientated Techniques. *Comp in Phys* 1998;12:620–630.
39. Ding J, Lyczkowski RW, Burge SW, Gidaspow D. Three-dimensional models of hydrodynamics and erosion in fluidized-bed combustors. *AIChE Symp Ser.* 1992;88:85–98.

Manuscript received Apr. 28, 2004, and revision received Apr. 19, 2005.